A Comprehensive Study on Carbon Dioxide Reforming of Methane over Ni/γ-Al2O3 Catalysts

ARTICLE *in* INDUSTRIAL & ENGINEERING CHEMISTRY RESEARCH · JULY 1999

Impact Factor: 2.59 · DOI: 10.1021/ie980489t

2 AUTHORS:

Shaobin Wang
Curtin University
271 PUBLICATIONS **9,312** CITATIONS
SEE PROFILE

Max Lu
University of Queensland
580 PUBLICATIONS **30,256** CITATIONS
SEE PROFILE

A Comprehensive Study on Carbon Dioxide Reforming of Methane over Ni/γ-Al_2O_3 Catalysts

Shaobin Wang and G. Q. (Max) Lu*

Department of Chemical Engineering, The University of Queensland, St. Lucia, Brisbane, Queensland 4072, Australia

Carbon dioxide reforming of methane into syngas over Ni/γ-Al_2O_3 catalysts was systematically studied. Effects of reaction parameters on catalytic activity and carbon deposition over Ni/γ-Al_2O_3 catalysts were investigated. It is found that reduced $NiAl_2O_4$, metal nickel, and active species of carbon deposited were the active sites for this reaction. Carbon deposition on Ni/γ-Al_2O_3 varied depending on the nickel loading and reaction temperature and is the major cause of catalyst deactivation. Higher nickel loading produced more coke on the catalysts, resulting in rapid deactivation and plugging of the reactor. At 5 wt % Ni/γ-Al_2O_3 catalyst exhibited high activity and much lesser magnitude of deactivation in 140 h. Characterization of carbon deposits on the catalyst surface revealed that there are two kinds of carbon species (oxidized and −C−C−) formed during the reaction and they showed different reactivities toward hydrogenation and oxidation. Kinetic studies showed that the activation energy for CO production in this reaction amounted to 80 kJ/mol and the rate of CO production could be described by a Langmuir−Hinshelwood model.

1. Introduction

The reforming reaction of methane with carbon dioxide (eq 1) into synthesis gas is a very attractive route for the production of energy and chemicals. This reaction is becoming an important area in CO_2 catalytic utilization because it offers several advantages over the process of steam reforming (eq 2) or partial oxidation of methane (eq 3). As discussed in the literature, most group VIII metals are catalytically active for this reaction, though deactivation of the catalyst by carbon deposition often occurred.[1−3] In industrial applications, nickel is more attractive due to its inherent availability and lower cost in comparison to noble metals. Several studies have shown that the nature of support employed influences the catalytic activity. Among the supports, such as Al_2O_3, SiO_2, TiO_2, MgO, ZrO_2, CeO_2, La_2O_3, clays, and zeolites, Ni/Al_2O_3 catalysts showed the highest initial activities. However, they suffer serious deactivation.[4−17]

$$CO_2 + CH_4 \rightarrow 2CO + 2H_2 \quad \Delta H_{298} = 247 \text{ kJ/mol} \quad (1)$$

$$CH_4 + H_2O \rightarrow CO + 3H_2 \quad \Delta H_{298} = 206 \text{ kJ/mol} \quad (2)$$

$$2CH_4 + O_2 \rightarrow 2CO + 4H_2 \quad \Delta H_{298} = -71 \text{ kJ/mol} \quad (3)$$

Several researchers have developed Ni-based catalysts such as Ni/MgO,[8,18] Ni/La_2O_3,[5,19] and Ni/ZrO_2[6] which could be effective catalysts for CO_2 reforming of methane in terms of conversion and stability. Seshan et al.[6] studied a series of Ni/ZrO_2 catalysts for CO_2 reforming of methane and found that catalysts with high nickel loading deactivated quickly because of coking. The 1−2 wt % Ni/ZrO_2 catalysts were more stable and showed reasonable good activities. Hu and Ruckenstein[18] researched Ni/MgO catalysts for CO_2 reforming of methane and found that Ni/MgO catalysts exhibited higher activities and coking resistance because of the formation of a NiO−MgO solid solution. Zhang and Verykios[5,19] reported that 17 wt % Ni/La_2O_3 catalysts would exhibit comparable activities to the initial activity of Ni/γ-Al_2O_3 after a reaction of 5 h and keep their activities as long as 120 h even at lower temperatures. However, Ni/MgO catalysts have to be activated at quite higher temperatures (above 800 °C) prior to the catalytic performance. La_2O_3 and ZrO_2 are not suitable as catalyst supports on a commercial scale because of their costs.

Carbon formation on Ni catalysts has been found to be the major cause of catalyst deactivation and reactor plugging. In addition, it was known that sintering of metallic Ni particles on a catalyst also caused catalyst deactivation. Gadalla and Bower[4] reported that the formation of $NiAl_2O_4$ spinel could be another mechanism for the deactivation of Ni/Al_2O_3 catalysts. However, some researchers demonstrated that the Ni/γ-Al_2O_3 catalyst could exhibit good stability at certain conditions.[7,15,17]

Xu et al.[7] investigated the catalytic activities of Ni/γ-Al_2O_3 catalysts and found that a 9.17 wt % Ni/γ-Al_2O_3 catalyst did not deactivate during 120 h of testing at 700 °C with a CO_2:CH_4 = 1.30:1 stream and that Ni/γ-Al_2O_3 catalysts of which the Ni loading was below 13.15 wt % showed high resistance to carbon deposition. Chen and Ren[17] reported that high-temperature calcination of Ni/γ-Al_2O_3 catalysts suppressed coke formation and the catalysts did not lose activities as long as 120 h. In our recent study, we found that a Ni/γ-Al_2O_3 catalyst showed not only high activity but also fairly good stability in 24 h.[15]

In this paper we reported more detailed studies on Ni/γ-Al_2O_3 catalysts. In this investigation, effects of several reaction parameters on catalytic activity were studied. The carbon species formed on the catalyst were characterized by XRD, XPS, TEM, TPH, and TPO (X-

* To whom all correspondences should be addressed. E-mail address: maxlu@cheque.uq.edu.au.

10.1021/ie980489t CCC: $18.00
Published on Web 05/29/1999

ray diffraction, X-ray photoelectron spectroscopy, transmission electron spectroscopy, temperature-programmed hydrogenation, and temperature-programmed oxidation, respectively), which will provide more insights into the role of carbon/coke formed in the CO_2 reforming of the methane reaction. The kinetics and reaction mechanism were also studied under differential conditions.

2. Experimental Section

2.1. Catalyst Preparation and Characterization. The catalysts were prepared using the wetness impregnation method. The support γ-Al_2O_3 (Aldrich) has a BET surface area of 190 m^2/g and pore volume of 0.214 mL/g. A $Ni(NO_3)_2$ (BDH) solution was used as a precursor. After evaporation, the catalysts were dried and calcined at 500 °C for 4 h in air.

The surface area and pore size distribution of the catalysts were determined by nitrogen adsorption, using an automatic surface and pore analyzer (Quantachrome, NOVA 1200). The samples were degassed at 300 °C in high vacuum before measurements. XRD analyses were carried out on a Phillips 1840 powder diffractometer, using Co Kα radiation. The nickel particle size was determined using Ni(111) reflectance and the Scherrer equation. XPS spectra were obtained on a ESCA PHI-560 system (Perkin-Elmer) using Mg Kα radiation. TEM investigations were performed on a JEOL 4000FX microscope. The samples were prepared under ethanol and suspended on a carbon film for examination.

TPH was also used to characterize the carbonaceous species formed on the catalyst surface after reaction. These experiments were conducted as follows: when the reforming reaction was performed for a certain period of time (1 h), the reactant stream was switched to N_2 flow to cool the aged catalyst to ambient temperature, and then TPH started from 50 to 800 °C at 5 °C/min under the mixture 10% H_2/N_2 with a flow rate of 30 mL/min, respectively. Gases were analyzed by gas chromatography (Shimadzu GC-17A).

TPO was conducted in a thermogravimetric analyzer (TGA) apparatus (Shimadzu TGA-50). A 5 mg sample was loaded in a Pt pan, heated from room temperature to 110 °C under the flow of air, kept at that temperature for 30 min, and then heated to 800 °C at 10 °C/min.

2.2. Catalytic Reaction. 2.2.1. Integral Reaction. The catalytic reforming reaction was carried out under atmospheric pressure in a flow system using a vertical quartz tube reactor. Typically, 0.2 g of catalyst was loaded on quartz wool. The molar ratio of the reactant stream was CO_2/CH_4 = 1:1 with a gas hourly space velocity (GHSV) of 18 000 $cm^3\ h^{-1}\ g^{-1}$. An internal thermocouple was located at the same level as the catalyst bed. The catalyst was reduced in 10% H_2/N_2 (30 mL/min) at 500 °C for 3 h, followed by an increase to reaction temperature at the rate of 20° C/min in N_2 prior to each catalytic reaction run. The product stream was analyzed by gas chromatography (Shimadzu GC-17A) using a thermal conductivity detector (TCD) for the detection of the reaction products. The methane and carbon dioxide gases used were of ultrahigh purity (>99.999%) obtained from Matheson, USA.

2.2.2. Differential Reaction and Kinetics. Then 1−5 mg catalysts were diluted with α-Al_2O_3 powder to make a 50 mg sample and loaded in a fixed-bed reactor. Conversions were usually controlled to be significantly lower than those defined by thermodynamic equilibrium (<5%). To determine the apparent activation energies, the reforming reaction was performed with a feed composition of CO_2:CH_4:He = 15:15:70 with a total flow rate of 360 mL/min over a temperature range of 500−700 °C. The partial pressure dependencies were studied by maintaining the pressure at 0.15 atm of one reactant and varying the other reactant between pressures of 0.02 and 0.15 atm. A balance gas of He was adjusted to maintain a total gas flow rate of 360 mL/min and a total absolute pressure of 1 atm. Calculations indicate that kinetic results obtained under these conditions were free of mass transfer.[20]

Table 1. Textural Variations of Ni Catalysts

catalyst	S_{BET} (m^2/g)	V (cm^3/g)	d (Å)
2 wt %	148	0.222	60.1
5 wt %	145	0.191	52.7
8 wt %	139	0.202	58.2
12 wt %	122	0.184	60.1
16 wt %	109	0.171	62.7
20 wt %	100	0.161	64.7

3. Results

3.1. Variations of Catalyst Texture and Structure. Table 1 shows BET surface areas, particle volumes, and average particle sizes of calcined catalysts with different Ni loadings. It can be seen that the surface area and pore volume decreased with increasing Ni loading. The crystalline phases of Ni/γ-Al_2O_3 investigated by X-ray diffraction (XRD) indicate that main phases of calcined and reduced catalysts are γ-Al_2O_3 and $NiAl_2O_4$, a compound resulting from the solid-state reaction between NiO and γ-Al_2O_3 in the Ni/γ-Al_2O_3 catalyst. The $NiAl_2O_4$, which has a stable spinel structure, is difficult to be reduced. However, the color difference can be observed between calcined and freshly reduced catalysts. The calcined sample was blue in color while the reduced catalyst had a bluish-black color. This suggests that the reduction was confined only to the surface layers and the spinel network remained intact after reduction.

3.2. Catalytic Activity of Supported Ni/γ-Al_2O_3 Catalysts. 3.2.1. Effects of Temperature and Space Velocity (F/W). Catalytic activity was investigated at temperatures of 500−800 °C, and the variations of CH_4 and CO_2 conversions at different nickel loadings and temperatures are shown in Figure 1. It is obvious that the conversions increased with increasing reaction temperature and nickel content. When the nickel loading was greater than 12 wt %, the conversion would reach the thermodynamic equilibrium. It is found that the CO_2 conversions were always higher than CH_4 conversions, which indicates that the reverse water−gas shift reaction occurred in the CO_2-reforming reaction.

The effect of space velocity on CH_4 conversion was investigated at 600 and 700 °C. As shown in Figure 2, CH_4 conversions were constant before a space velocity of 2×10^4 mL/g·h and decreased as the space velocity increased at both temperatures. The decrease in CH_4 conversion at a high space velocity was due to less contact time between the reactants and the catalyst.

3.2.2. Catalyst Stability in the Integral Reaction. The temperature dependence of the deactivation process was investigated under 600 and 700 °C over a 5 wt % Ni/γ-Al_2O_3 catalyst. As clearly shown in Figure 3, CH_4 and CO_2 conversions decreased faster in 1−5 h and then

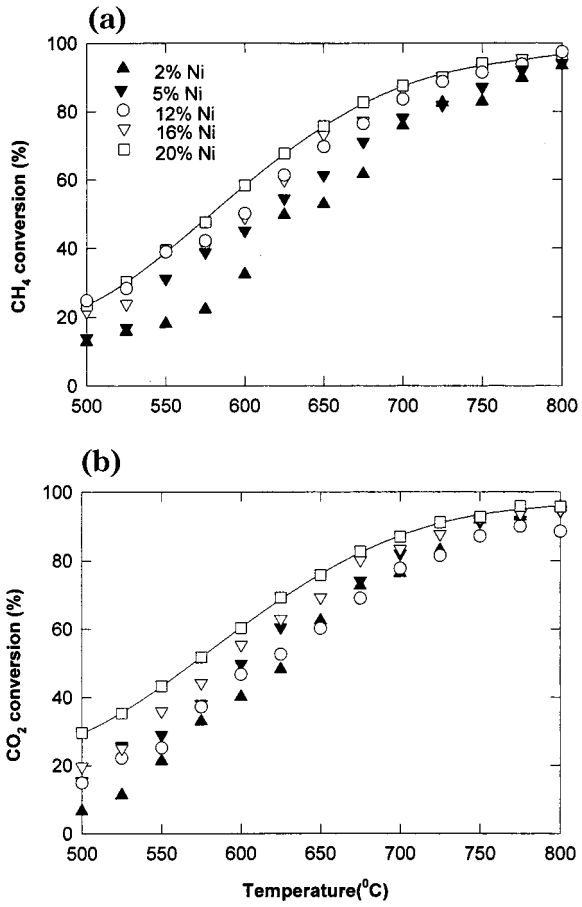

Figure 1. CH_4 and CO_2 catalytic conversions over various Ni/γ-Al_2O_3 at 500−800 °C. Reaction conditions: CH_4:CO_2 = 1:1, P = 1 atm, F/W = 18 000 mL/h·g_{cat}.

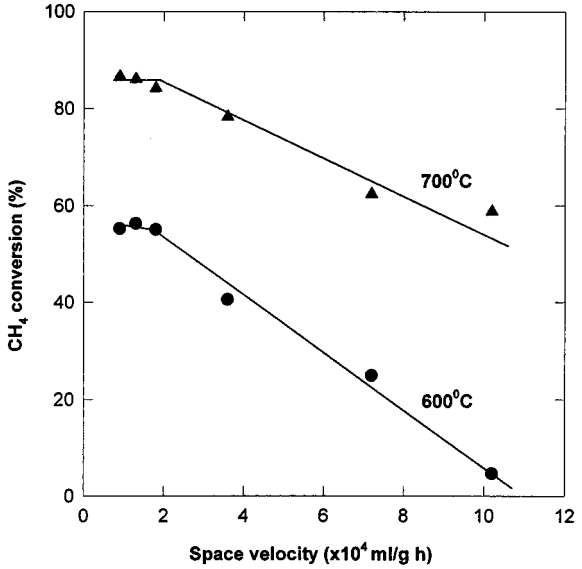

Figure 2. Effect of space velocity on CH_4 conversion at 600 and 700 °C.

the variation of conversion tends to decrease either at 600 or 700 °C. At 600 °C, CH_4 and CO_2 conversions declined from the initial 38% and 49% to 23% and 33%, respectively, after 70 h. In the case of 700 °C, CH_4 and CO_2 conversions decreased from 73% and 81% to 58% and 65%, respectively, in 140 h. It is noted that after 20 h the decreases in conversions over a 5 wt % Ni/γ-Al_2O_3 catalyst were not significant. TGA measurements demonstrated that carbon deposition on a 5 wt % Ni/

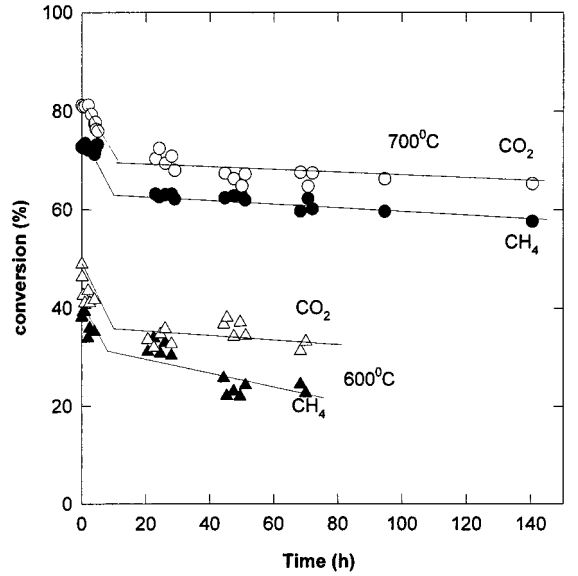

Figure 3. Effect of temperature on the deactivation of 5% Ni/γ-Al_2O_3 catalysts. Reaction conditions: CH_4:CO_2 = 1:1, P = 1 atm, F/W = 18 000 mL/h·g_{cat}.

Table 2. Carbon Deposition on Various Catalysts

	coke (%)	
catalyst	600 °C	700 °C
2 wt % Ni/γ-Al_2O_3		0.43[a]
5 wt % Ni/γ-Al_2O_3	8.01[a]	14.3[b]
8 wt % Ni/γ-Al_2O_3		48.32[a]
12 wt % Ni/γ-Al_2O_3		62.76[c]

[a] 70 h. [b] 140 h test. [c] 2 h test.

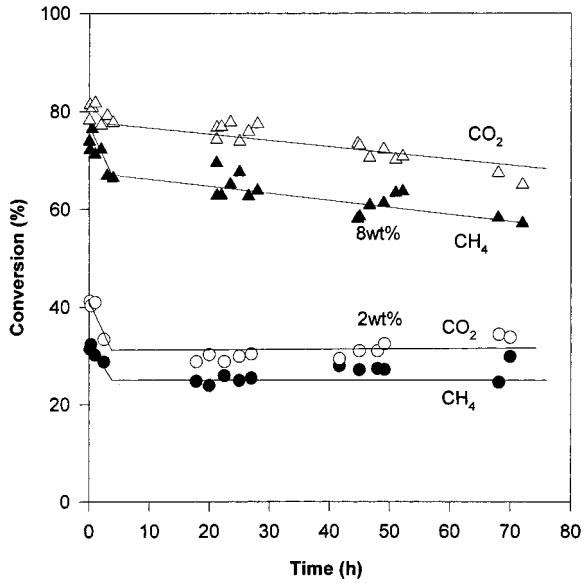

Figure 4. Stability testing of Ni/γ-Al_2O_3 with various Ni loadings catalysts at 700 °C. Reaction conditions: CH_4:CO_2 = 1:1, P = 1 atm, F/W = 18 000 mL/h·g_{cat}.

γ-Al_2O_3 catalyst at 700 °C was higher than that at 600 °C (Table 2). TGA investigations on carbon deposition showed that the coking rate on Ni/Al_2O_3 catalysts increased with increasing temperature and reached the highest value at 700 °C because of CH_4 cracking.[20] In addition, a longer reaction time-on-stream at 700 °C made more carbon deposit accumulate on catalysts.

Figure 4 shows the variations in CH_4 and CO_2 conversions, obtained at 700 °C over Ni/γ-Al_2O_3 catalysts with varying Ni loading, as a function of time-on-

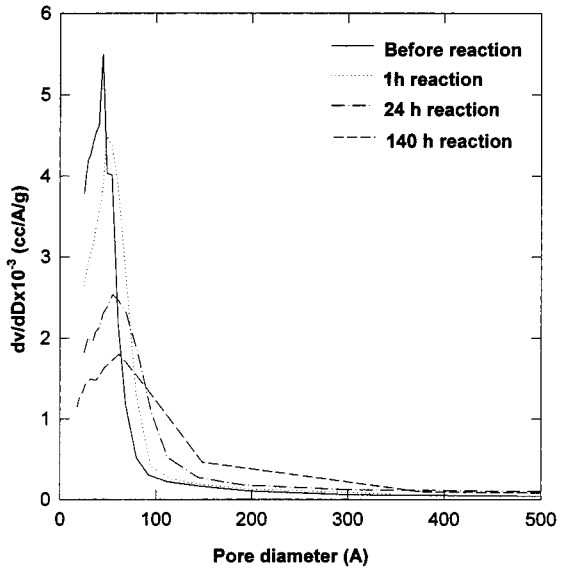

Figure 5. Pore size distributions of 5% Ni/γ-Al_2O_3 catalysts before and after reaction at 700 °C.

Table 3. Characteristics of 5 wt % Ni/γ-Al_2O_3 Catalysts before and after Reaction

catalyst	S_{BET} (cm^3/g)	V (cm^3/g)	d (A)	D_{Ni} (nm)	coke (%)
fresh	156	0.212	54.6		
1 h	140	0.214	61.1	10.7	3.3
24 h	105	0.240	91.7	16.6	13.4
140 h	90	0.244	95.3	14.6	14.3

stream. It is shown that Ni/γ-Al_2O_3 catalysts all showed some deactivation. Like the behavior of the 5 wt % Ni/γ-Al_2O_3 catalyst, 2 and 8 wt % Ni/γ-Al_2O_3 catalysts deactivated quickly in 1−5 h and then the rates were slowed. For 2 wt % Ni/γ-Al_2O_3, CH_4 and CO_2 conversions remained constant while 8 wt % Ni/γ-Al_2O_3 showed linear deactivation after 5 h. In the case of the 12 wt % Ni/γ-Al_2O_3 catalyst it was found that the reaction had to be stopped because of the reactor becoming completely plugged by carbon deposits after 2 h. The amount of carbon on Ni/γ-Al_2O_3 showed that the catalyst with higher nickel loading incurred more carbon deposition at the same temperature (Table 2).

3.2.3. Evolution of Catalyst Pore Structure. The parameters of the porous structure for 5 wt % Ni/γ-Al_2O_3 catalysts reacted at 700 °C for a certain period of time are given in Table 3. It is seen that the surface area was recovered after reduction comparing to that of the sample as prepared (Table 1). However, it decreased upon reaction and the reduction increased with increasing reaction time, whereas the pore volume and average pore size showed an increasing trend. The characterization of the catalysts showed that most reduction occurred on the catalyst surface. N_2 adsorption would possibly be enhanced on the reduced $NiAl_2O_4$ catalyst. However, carbon deposits would prevent N_2 adsorption on the catalyst surface. The pore size distributions (Figure 5) showed that the peak became more and more broad and peak maximums were shifted to a large pore range after reaction. These indicate that the pores were gradually blocked by the deposited carbon.

3.2.4. XRD, XPS, and TEM Studies of Carbon Deposits. XRD patterns of fresh and used 5 wt % Ni/γ-Al_2O_3 catalysts after reaction at 700 °C are presented in Figure 6. It is seen that no nickel diffraction peaks appeared on the fresh catalyst. After 1 h reaction-weak nickel diffraction occurred but no graphite can be

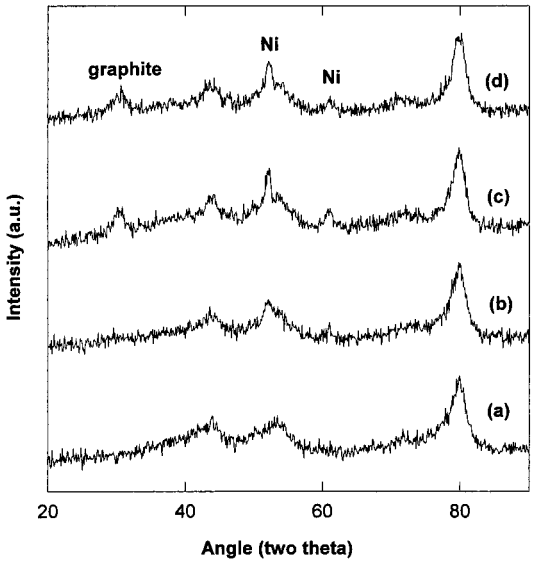

Figure 6. XRD patterns of 5% Ni/γ-Al_2O_3 before and after reaction: (a) reduced, (b) 1 h of reaction, (c) 24 h of reaction, and (d) 140 h of reaction.

Table 4. XPS Results of Surface Elements on Various Nickel Catalysts

catalyst	C (%)	O (%)	Al (%)	Ni (%)
fresh	5.04	61.76	31.85	1.35
reacted 1 h	25.60	47.34	26.38	0.68
reacted 24 h	56.63	27.96	15.01	0.40
reacted 140 h	57.44	26.93	15.20	0.42

detected. Nickel (2θ = 52.4° and 60.9°) and graphitic carbon (2θ = 30.5°) peaks occurred on catalyst XRD patterns after 24 and 140 h of reaction. However, the peak intensities are about the same for the two samples. The variations of nickel particle sizes and carbon contents on catalysts are given in Table 3. The Ni particle size generally decreases as the reaction time is prolonged. After 24 h the nickel particle size and coking were about the same.

XPS results may give more information on the variations of the catalyst surface after reaction. The chemical compositions of fresh and used catalysts are given in Table 4. It is seen that surface carbon species existed on the fresh catalyst. This is due to the exposure of the catalyst to air. CO_2 can be adsorbed on Ni/γ-Al_2O_3 catalysts. Aluminum, oxygen, and nickel concentrations all decreased because of the coverage of carbon when catalysts reacted on stream. The ratio of O:Al was larger than expected (3:2) because of the coverage of carbon layers. After 1 h of reaction carbon concentration accounted for one-quarter of the surface components and it increased to more than 50% after 24 h. For a prolonged period of time (140 h), the carbon concentration did not increase further. In contrast, surface Ni concentration decreased one-half of its initial concentration after 1 h of reaction, the reduction was even smaller at 24 h, and the concentration kept nearly constant afterward.

C 1s spectra over 5 wt % Ni/γ-Al_2O_3 reacted over different times are shown in Figure 7. It is seen that two carbon species are generally formed on the catalyst surface. Before reaction only one peak can be seen in the C 1s spectra. After reaction for 1 h the peaks corresponding to graphitic carbon (−C−C− with a binding energy (BE) of 284.5 eV) and oxidized carbon species (−C−CO−, BE = 285.9 eV and CO_3^-, BE =

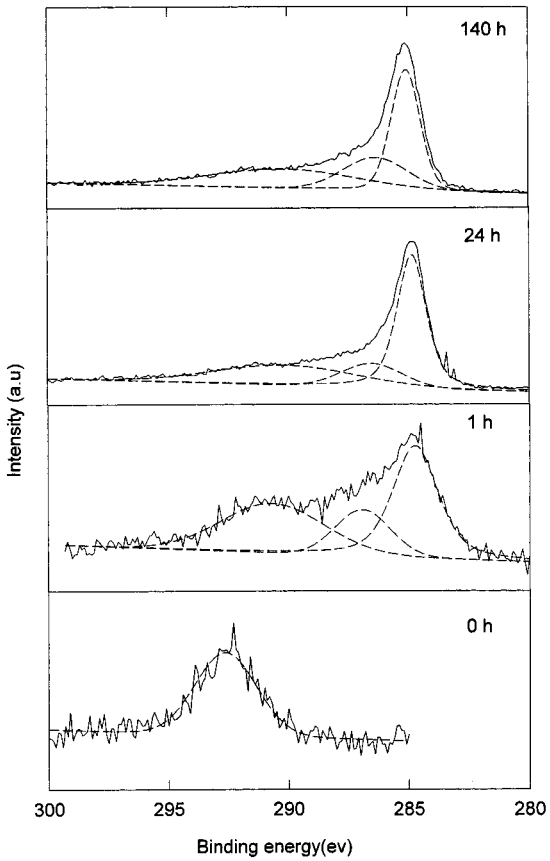

Figure 7. XPS C 1s spectra of 5% Ni/γ-Al_2O_3 before and after reaction: (a) reduced, (b) 1 h of reaction, (c) 24 h of reaction, and (d) 140 h of reaction.

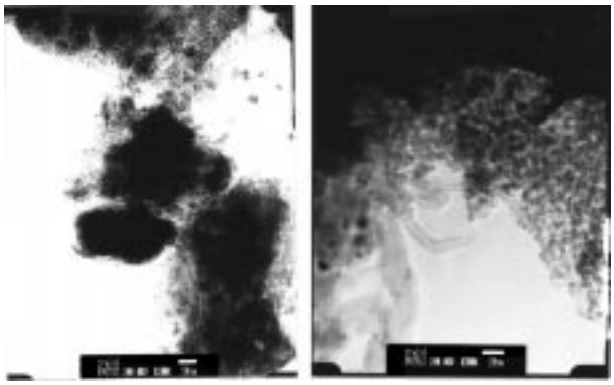

Figure 8. TEM pictures of 5% Ni/γ-Al_2O_3 catalysts before and after reaction, (a) reduced and (b) 24 h of reaction.

289.8 eV) appeared. After 24 h of reaction the intensities of graphite increased a great deal which suggested that much more graphite formed on the catalyst surface. However, there was little difference between the C 1s spectra for 24 h of reacted catalyst and the one for 140 h of reaction.

TEM was used to characterize the morphologies of fresh and reacted catalysts. As shown in Figure 8, the fresh catalyst presented a layered phase deposited on the γ-Al_2O_3 support, characteristic of $NiAl_2O_4$. No forms of carbon are visible. After 24 h of reaction a number of heterogeneous particles are detected. Many hollow graphitic fibers of typically 10 nm in diameter can be observed.

3.2.5. TPH and TPO Studies of Carbon Deposits. In order to characterize the carbonaceous species formed during the reforming reaction of methane with CO_2 at

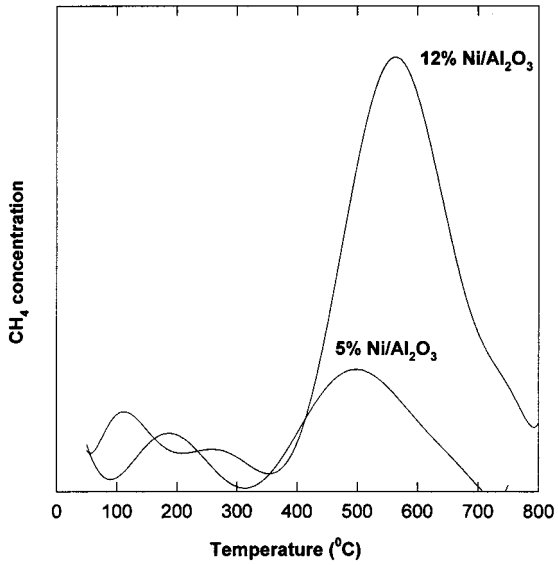

Figure 9. TPH profiles of carbonaceous species on 5% Ni/γ-Al_2O_3 and 12% Ni/γ-Al_2O_3 catalysts.

700 °C, TPH and TPO experiments were carried out after the reaction on various catalysts. The results of TPH over 5 wt % Ni/γ-Al_2O_3 and 12 wt % Ni/γ-Al_2O_3 catalysts after 1 h of reaction are shown in Figure 9. It is seen that two broad peaks of methane were observed on TPH spectra over the two catalysts. The first peak occurred between 100 and 250 °C and the maximum temperature of the second broad peak appeared around 500 and 570 °C for 5 wt % Ni/γ-Al_2O_3 and 12 wt % Ni/γ-Al_2O_3 , respectively. It is noted that the intensity of the high-temperature peak increased greatly on the 12 wt % Ni/γ-Al_2O_3 TPH profile. The TPH results indicate that three types of carbonaceous species existed on the catalysts. The first two types of carbonaceous species were very active toward hydrogenation. The third kind of carbon deposits could not react to produce CH_4 until 400 °C. Peaks of carbon hydrogenation on 5 wt % Ni/γ-Al_2O_3 generally occurred earlier than those on 12 wt % Ni/γ-Al_2O_3. This suggests that the greater amount of nickel loading, the more aged carbon deposits produced and less active toward hydrogenation. It is also noted that the amount of carbon at low temperatures was different on two catalysts. The higher amount of active carbon on 12 wt % is probably due to the higher Ni laoding, which could produce more CH_4 cracking on Ni sites.

The oxidation of carbonaceous species to CO_2 over 5 wt % Ni/γ-Al_2O_3 after a certain period of reaction time-on-stream at 700 °C is presented in Figure 10. TPO profiles also demonstrated oxidation of carbonaceous species, which started at 500 °C. The oxidation rate reached its maximum around 670 °C for catalysts that reacted for 1 h. The peak temperature shifted a bit to a higher temperature when the catalyst reacted for a longer period of time. This seems to show that the amount of less active carbon toward oxidation formed on the catalyst was enhanced for a longer period of time-on-stream. Activation energies for the oxidation of carbon species on catalysts were calculated on the basis of the Haines method[21] (see Table 5). The activation energy of TPO for carbon deposits on Ni/γ-Al_2O_3 after 1 h of reaction could be derived over the whole temperature range, whereas for other cases activation energies were obtained over two temperature ranges of 500−600 and 600−700 °C. For the same reacted catalyst, the

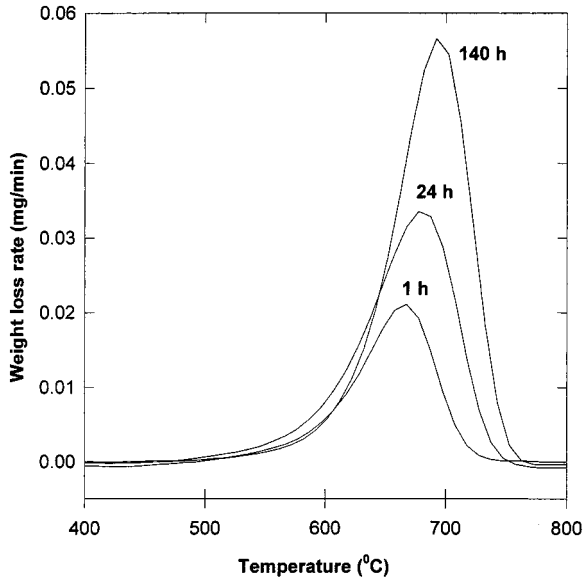

Figure 10. TPO profiles of carbonaceous species on 5% Ni/γ-Al_2O_3 after reaction at 700 °C.

Table 5. Activation Energies of Carbon Oxidation on 5 wt % Ni/γ-Al_2O_3 Catalysts

time	T (°C)	E_a (kJ/mol)
1 h	500−720	216
24 h	510−600	153
	600−700	262
140 h	520−600	168
	600−700	282

activation energy at higher temperatures was much greater than that at lower temperatures. In the same temperature range the activation energy of TPO for 140 h of reacted Ni/γ-Al_2O_3 was higher than that for the catalyst reacted for 24 h. These results seem to suggest that carbon species on the catalyst that reacted for 140 h were more difficult to be oxidized, and the second stage for carbon oxidation required higher energy to induce the reaction.

3.2.6. Kinetic Studies. The dependency of the reaction rate on temperature was measured at 500−700 °C. The relationships between the initial reaction rate for CH_4 and CO_2 consumptions as well as CO production versus temperature over 5 wt %Ni/γ-Al_2O_3 were shown in Figure 11. The apparent activation energies obtained are listed in Table 6. Because of the insensitivity of the TCD to H_2 with He as the carrier gas, the detection of a lower concentration of H_2 is very difficult and much larger errors would incur. Hence, no activation energy for H_2 formation was obtained.

It is seen that the activation energy for CO production was about 80 kJ/mol. CO_2 consumption showed higher activation energy for CH_4 consumption, and they were all lower than that for CO production. The lower apparent activation energies for CH_4 or CO_2 consumption suggests that the rate-determining step for CO formation is probably different from those of CH_4 and CO_2 consumptions. This phenomenon differs from the results reported by Bradford and Vannice.[22] In their work, it was found that the apparent activation energies for all gas reactions were similar, in the range of 80−100 kJ/mol. However, the activation energies for CH_4 consumption were about 33 kJ/mol for all Ni catalysts tested, according to the work done by Osaki et al.[23] Therefore, our results are the medium of those two values.

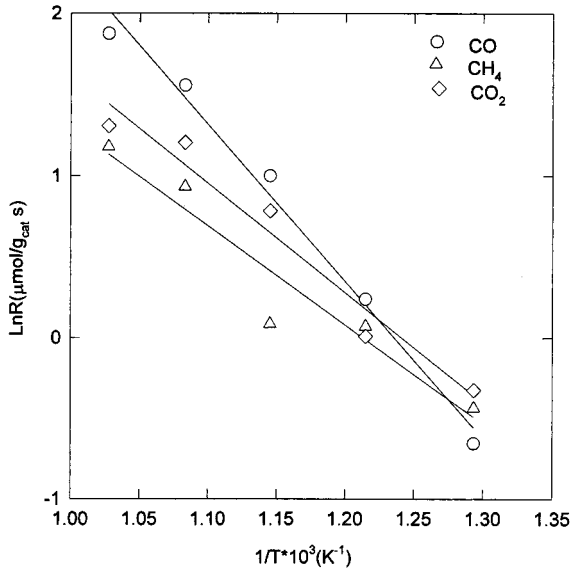

Figure 11. Arrehenius plots for CH_4 and CO_2 consumptions and CO production.

Table 6. Activation Energies for CH_4−CO_2 Reaction

catalyst	E_{CO} (kJ/mol)	E_{CH_4} (kJ/mol)	E_{CO_2} (kJ/mol)
Ni/γ-Al_2O_3	80.5	50.9	56.1

The dependencies of the rate of CO production on the feed partial pressure of CH_4 and CO_2 were determined in a broad temperature range and were plotted in Figure 12. As shown, a linear relationship between the CO production rate and CH_4 partial pressure was observed, while the relationship between the CO production rate and CO_2 partial pressure varied, depending on the range of CO_2 pressure. At lower partial pressures (<6 kPa), the reaction rate increased as the pressure increased. At higher partial pressures, the rate remained almost constant.

The reaction orders for CH_4 and CO_2 were determined from a simple power law equation by linearization of a logarithmic plot:

$$R_{CO} = kP_{CH_4}^{a}P_{CO_2}^{b} \quad (4)$$

Table 7 gives a summary of the determined reaction orders. It is seen that the reaction order for CH_4 was close to first-order at all temperatures for both catalysts. The reaction order for P_{CO_2} approached zero at high partial pressures (>6 kPa). These results are in agreement with those of Rostrup-Nielsen and Hansen.[24] They reported a zero-order dependence in P_{CO_2}, as well as a first-order dependence in P_{CH_4} in CO_2 reforming over Ni/Mg(Al)O. Olsbye et al.[25] also reported similar results for a Ni/La_2O_3−Al_2O_3 catalyst in CO_2−CH_4 reforming at the temperatures of 700−900 °C. Takano et al.[26] found similar results over Ni/Al_2O_3 for this reaction. For CO_2 partial pressure lower than 8.4 kPa, the reaction order for P_{CO_2} is almost 1; for CO_2 pressure in the range of 8.4−67.6 kPa, the order is zero.

4. Discussion

4.1. Catalytic Performance of Ni/γ-Al_2O_3 Catalysts. The XRD patterns indicated that after the reduction of the Ni/γ-Al_2O_3 catalyst at 500 °C no nickel particles are detected. This can be attributed to the formation of $NiAl_2O_4$ spinel from NiO and Al_2O_3 sup-

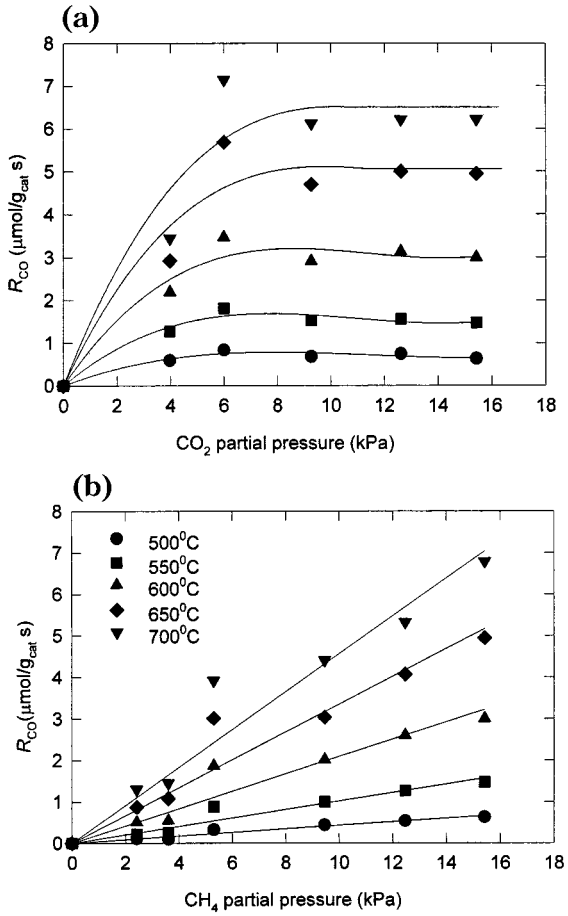

Figure 12. Relationship between the CO production rate and CH_4 or CO_2 partial pressure.

Table 7. Reaction Orders Based on Simple Power Law

	Ni/Al_2O_3	
temp (°C)	CH_4	CO_2[a]
500	1.05	0.83
550	1.08	0.85
600	1.00	1.11
650	0.93	1.61
700	0.90	1.77

[a] $P_{CO_2} < 6$ kPa.

port, which is very difficult to be reduced at 500 °C. The other reason may be a lesser amount of nickel metal and higher dispersion. Nickel crystallites having diameters of less than 3 nm cannot be observed by XRD. It is generally proposed that Ni particles are the active sites for CO_2 reforming of methane and $NiAl_2O_4$ is inactive. However, in this investigation it is shown that the Ni/γ-Al_2O_3 catalyst has much higher initial catalytic activity and long-term stability. Therefore, it is believed that some other species acting as active sites for the reforming of methane on Ni/γ-Al_2O_3 besides Ni crystallites. The active species could be partly reduced $NiAl_2O_4$.

Al-Ubaid et al.[27,28] reported that a catalyst having a composition corresponding to $NiAl_2O_4$ after reduction showed the highest activity for the steam reforming of methane. Murthy and Swamy[29] also found that reduced $NiAl_2O_4$ exhibited dehydrogenation activity. Lunsford et al.[30] reported that $NiAl_2O_4$ exhibited moderate activity in methane partial oxidation and proceeded phase transformation at different catalyst regions, resulting in varying activity. Recently, Chen and Ren[17] have studied the effects of calcination temperature on catalytic activity over a series of Ni/γ-Al_2O_3 catalysts, and their observations indicated that the formation of surface spinel $NiAl_2O_4$ has a positive effect on the suppression of carbon deposition and that the calcined $NiAl_2O_4$ spinel phase is not active in a reforming reaction but its reduced form can lead to significant activity and stability. Gadalla and Bower[4] tested 12−14 wt % Ni catalysts supported on Al_2O_3−MgO and found that despite the loss of Ni sites to form the spinel solid solution ($NiAl_2O_4$) in the reaction no corresponding loss in activity was evidenced, a result suggesting that the new phase formed was more active than metallic nickel.

As the catalytic reaction proceeds, some of the $NiAl_2O_4$ would be reduced to Ni under the reaction atmosphere. XRD patterns have shown the evolution of Ni particles during the reaction process (Figure 6). The reduction of nickel aluminate in the reaction and sintering of nickel increased with increasing time. However, it would stop after a certain period of time. XPS spectra indicated that there were still some nickel species (one-third of the initial concentration) on the catalyst surface. Chen and Shiue[31] studied the reduction of nickel aluminate catalysts and observed that reduction of Ni/γ-Al_2O_3 to the Ni metal increased much more with time at the initial period of reduction but increased little with time at the final period of reduction. Dispersion decreased as time increased at the same temperature.

Stability testing has demonstrated that the Ni/γ-Al_2O_3 catalyst could show long-term stable CO_2 and CH_4 conversions, although carbon deposition on the catalyst is high. This suggested that some carbon species formed on the surface of catalysts must be involved in the reaction to produce CO (i.e., acting as active sites in the reaction but not as a deactivating factor). Our research on the effect of support on Ni-based catalysts has shown that Ni/α-Al_2O_3 and Ni/La_2O_3 catalysts have higher activity despite serious carbon deposition.[15] This is probably due to the higher reactivity of carbon species on the catalyst surface. Zhang et al.[32] studied the effect of support on reactivity over Rh-based catalysts and found that a significant amount of carbon is formed during the reaction over Rh/γ-Al_2O_3, but this catalyst exhibited a high turnover frequency (TOF) value as compared to the other supported Rh catalysts. Steady-state tracing experiments showed that a large amount of active carbon participated in the sequence of steps to form CO over the Rh/Al_2O_3 while over other catalysts it was practically immeasurable.[32] York et al.[33] recently reported that Mo and W carbides are extremely active and stable catalysts for this reaction. Thus, some researchers proposed that the actual active phase for reforming is not the metal itself but a carbided form of the metal, or even surface carbon atoms.[34−37]

The nickel loading on a catalyst greatly influenced the catalytic activity and the amount of carbon deposition, in turn leading to the different magnitude of catalyst deactivation. Stability tests demonstrated that the greater amount of nickel loading, the faster the catalyst deactivation. Because of a much higher coking rate Ni/γ-Al_2O_3 catalysts with nickel loading over 12 wt % would quickly plug the reactor in 5 h. Carbon deposition comes from two routes: CH_4 decomposition and CO disproportionation. The increase in nickel content increased the decomposition of CH_4 and also CO disproportionation, resulting in an increase in carbon deposition (Table 2). In our research on carbon deposi-

tion in this reaction using the TGA technique, it is also found that carbon deposition on 12 wt %Ni/Al_2O_3 reached 140% after 2 h while it was only 20% on 5 wt % Ni/Al_2O_3.[20] Ruckenstein and Hu[9] reported that the relatively small amount of carbon deposited over 1 wt % Ni/Al_2O_3 during the CH_4-CO_2-reforming reaction explained the slow decrease in activity with time. Instead, over a 13.6 wt % Ni/Al_2O_3 catalyst the carbon deposition was so fast that the reactor was plugged in 6 h. Lercher et al.[38] also found that the Ni/ZrO_2 catalyst containing the high Ni loading deactivated rapidly, while the one with low Ni loading was remarkably stable.

Therefore, it could be concluded on the basis of the previous discussions that nickel crystallites and the reduced nickel aluminate were the initial active sites. As the reaction proceeded, more nickel particles and Ni−C intermediates would also act as the active sites for CO_2 reforming of methane over Ni/γ-Al_2O_3 catalysts. However, the specific roles of each type of active sites in the reaction are not clear at present. Further research is desired in this aspect. The deactivation of the Ni/γ-Al_2O_3 catalyst can be ascribed to carbon deposition and nickel sintering. If the rate of carbon deposition is higher than the rate of gasification of the carbon formed, fast deactivation of the catalyst would result.

4.2. Chemical Structure of Carbon Deposits and Their Reactivities. Carbon deposition is a major problem in methane reforming with carbon dioxide. Carbon deposition can cause catalyst deactivation and reactor plugging. Understanding of the chemical and morphological properties of carbon deposits help us to know how they influence catalytic activity and stability of the catalysts.

In this work, XPS characterization demonstrated the existence of mainly two kinds of carbon species, graphitic and oxidized carbons. XRD patterns show that carbon formed on a 5 wt % Ni/γ-Al_2O_3 catalyst after 1 h of reaction dispersed well and could not be observed. For longer reaction times, mainly graphitic carbon formed. TEM micrographs show that the carbon on Ni/γ-Al_2O_3 after 24 h is filamentous carbon. Hence, it is concluded that filamentous carbon having a graphitic structure dominated the carbon species on the Ni/γ-Al_2O_3 catalyst. Chen and Ren[17] used TEM to observe the growth of filamentous carbon during the reforming reaction over Ni/γ-Al_2O_3 where Ni particles are on the tip of the carbon filaments. Mikhailova et al.[39] also reported that formation of the filamentous carbon was accompanied by the destruction of a catalyst and embedding of its particle into the structure of the carbon filaments in the methane reaction with carbon dioxide over Ni/γ-Al_2O_3.

TPH studies indicated that three types of carbon deposits formed on Ni/γ-Al_2O_3 and their amounts were dependent on the Ni loading. A larger amount of inactive carbon toward hydrogenation formed on the 12 wt % Ni/γ-Al_2O_3 catalyst, resulting in its quicker deactivation and full plugging of the reactor. XPS results demonstrated that surface carbon deposits consisted of −C−C− and oxidized carbon species (−C−CO, CO_3^-). The −C−C species is in the form of filaments and oxidized carbons are possible presented in amorphous carbon. Bokx et al.[40] found that amorphous carbon deposited on Ni/SiO_2 via CH_4 decomposition was more reactive for H_2 gasification than filamentous carbon. Shi et al.[41] reported that most of the deposited carbon from CH_4 dissociated on the Ni/Al_2O_3 catalyst could be gasified by CO_2. However, there were still some carbon that could not be gasified. It generally deposited on the support. They proposed that carbon gasification only happened on the interface between carbon filaments and the metal particle. It is known that hydrogen atoms are formed on the metal surface via dissociation steps of gaseous H_2. Gasification of carbon species will proceed faster on carbon connected to metal particles. Therefore, it is deduced that the lower temperature peaks of TPH can be ascribed to the amorphous carbon and some of the filamentous carbon connected to the metal particle. The higher temperature peak is attributed to the filaments connected to the support.

TPO in this investigation revealed that carbon oxidization can be ascribed to one mechanism for the 1 h reacted catalyst, but two types of carbon oxidization mechanisms occurred for 24 and 140 h reacted catalysts. Goula et al.[42] reported that two distinct CO_2 peaks were observed in TPO profiles for $Ni/CaO-Al_2O_3$ catalysts and that a higher temperature peak of CO_2 in TPO was assigned to graphitic forms of carbon. Swaan et al.[43] conducted isotopic TPO experiments for the carbon deposits on Ni/SiO_2 catalysts in the CO_2 reforming of methane reaction and found that two kinds of carbon deposited on the catalysts. The first type of carbon oxidized at low temperature might be of the Ni_3C form originated from methane dissociation and accumulated during the initial stage of the reaction. The second type of carbon oxidized at high temperatures arose from the Boudouard reaction, and this carbon could progressively encapsulate the nickel particles. On the basis of this work it can be deduced that graphitic carbon grown at the early stage of reaction could be the filaments with the nickel particle on the top which had lower activation energy. The filaments with nickel particles encapsulated would be oxidized at higher temperatures.

The mechanism of filamentous carbon growth under the steam-reforming reaction has been studied.[44−46] Kroll et al.[35] proposed a similar mechanism for the formation of hollow filaments in the CO_2 reforming of methane. However, there are two processes that occurred, depending on the pretreatment of the catalysts. For calcined samples the reaction conditions would favor carbon migration without particle encapsulation, which is the case where no deactivating carbon formed. In contrast, in the case of prereduced samples, carbon growth is expected to proceed in all directions around the particle, rapidly forming a diffusion barrier to reactants and products, thus leading to the progressive isolation of the active surface from the reactant mixture. This is the highly deactivating encapsulating carbon.

Baker[47] found that the interaction between the metal catalyst particle and the supporting medium would influence the filament growth mode. The strong interaction resulted in the formation of filaments by the extrusion mode. In contrast, filaments grew by the conventional or whiskerlike mode on a weak metal/support interaction.

In this investigation, the Ni/γ-Al_2O_3 catalyst was not found reduced to Ni particles. The main phases of Ni/γ-Al_2O_3 catalysts are γ-Al_2O_3 and $NiAl_2O_4$, which has a spinel structure. Hence, the reaction conditions for Ni/γ-Al_2O_3 favor the formation of hollow filamentous carbon. The XPS and TEM results have verified this mechanism. This is the main reason, we believe, that

the 5 wt % Ni/γ-Al_2O_3 has very high conversion and long-term stability despite coke formation.

4.3. Reaction Mechanism and Model. Several researchers have studied the mechanism of CH_4 reforming of methane with carbon dioxide over supported nickel catalysts. It is generally believed that the most probable slow steps are those of methane activation to form CH_x ($x = 0-3$) and the reaction between CH_x species and the oxidant, either in the form of oxygen adatoms originating from CO_2 dissociation or CO_2 itself (including CO_2 activation). However, the results reported in the literature are not consistent, depending on reaction conditions. Zhang and Verykios[48] found that methane activation is the rate-determining step for the formation of synthesis gas over the Ni/La_2O_3 catalyst, while the reaction between surface carbon species (CH_x, $x = 0$) and the oxidant (including CO_2 activation) is the rate-determining step over the Ni/γ-Al_2O_3 catalyst. Wang and Au[49] studied the isotopic effects of CH_4/CD_4 in the carbon dioxide reforming of methane to syngas over the Ni/SiO_2 catalyst and concluded that CH_4 dissociation is the rate-determining step and CO_2 dissociation occurs prior to surface reaction of CH_x fragments. However, investigations conducted by Slagtern et al.[50] show that the reaction between surface carbon species from methane cracking and oxygen-adsorbed species resulted from CO_2 dissociation is rate-determining in the case of Ni/SiO_2. Osaki et al.[23] employed pulsed surface reaction analysis (PSRA) to probe the mechanism of CO_2 reforming of methane on supported nickel catalysts (Ni/SiO_2, Ni/MgO, Ni/Al_2O_3, and Ni/TiO_2). It was found that two reaction steps are responsible for H_2 production, that is, dissociative CH_4 adsorption to form CH_x species and the subsequent surface reaction of CH_x and CO_2 (or O), the rate-determining step. Bradford and Vannice[22] reported the reaction kinetics of CO_2-CH_4 reforming over various nickel catalysts and proposed a reaction model based on CH_4 activation to form CH_x and CH_xO decomposition as slow kinetic steps. Recently, Aparicio[51] studied the kinetics of elementary surface reactions involved in the reforming of methane to synthesis gas over supported nickel using transient isotopic methods. The model developed suggested that there is no single rate-determining step in methane reforming with either steam or CO_2, and that under some conditions the availability of surface oxygen may play a key role in determining the rate. Hu and Ruckenstein[52,53] employed a transient response analysis to study the reaction mechanism over Ni/SiO_2 and Ni/MgO, and they found that the surface reaction between C and O species constitutes the rate-determining step of the reforming reaction.

Most groups who reported kinetic studies of the CO_2-reforming reaction have proposed a Langmuir–Hinshelwood-type mechanism with an undefined number of H atoms in the intermediate CH_x species and with dissociative adsorption of CO_2.[24,54] Zhang and Verykios[55] have derived a rate expression in a Langmuirian model assuming that methane dissociation was the rate-determining step. The results reported by Olsbye et al.[25] showed that the experimental data were consistent with either a Langmuir–Hinshelwood mechanism, in which the surface reaction is the rate-determining step, or an Eley–Rideal-type mechanism, in which the reaction between CH_x and $CO_{2,g}$ is rate-limiting at low P_{CO_2} while adsorption of CH_x is rate-limiting at high P_{CO_2}. Various rate models were employed to fit the experimental data.[56] The best agreement was obtained with a rate model based on the stepwise mechanism, where in the rate-determining step methane is decomposed to hydrogen and active carbon followed by the direct and fast conversion of this active carbon with CO_2 to 2CO.

In this investigation, it has been shown that the activation energy for CO production is higher than that for either the CH_4 or CO_2 reaction. The lower activation energies for CH_4 or CO_2 consumption may suggest that these two gases first involved chemisorption in the reaction and the CO formation step is the rate-determining step. On the basis of the investigation and previous research, the mechanism can be simplified as follows:

$$CH_4 + * \rightarrow CH_4* \tag{5}$$

$$CO_2 + * \rightarrow CO_2* \tag{6}$$

$$CH_4* \rightarrow CH_3* + H \tag{7}$$

$$CH_3* \rightarrow CH_2* + H \tag{8}$$

$$CH_2* \rightarrow CH* + H \tag{9}$$

$$CH* \rightarrow C* + H \tag{10}$$

$$C* + CO_2* \rightarrow 2CO + 2* \tag{11}$$

$$CO \rightarrow C + O \tag{12}$$

$$2H + O \rightarrow H_2O \tag{13}$$

$$H + H \rightarrow H_2 \tag{14}$$

According to the dependencies of the reaction rate on CH_4 or CO_2 partial pressure, methane showed first-order and CO_2 exhibited first-order at lower partial pressures and zeroth order at high pressures. This phenomenon is similar to the work reported by Olsbye et al.[25] On the basis of their work, the rate expression in a Langmuir–Hinshelwood mechanism can be used to describe the CO_2-reforming reaction.

$$r = \frac{k_1 P_{CH_4} P_{CO_2}}{(1 + K_1 P_{CH_4})(1 + K_2 P_{CO_2})} \tag{15}$$

At a fixed CH_4 partial pressure, if P_{CO_2} is higher, that is, $K_2 P_{CO_2} \gg 1$, eq 15 is approximated by

$$r = \frac{k_1' P_{CH_4}}{1 + K_1 P_{CH_4}} \frac{k_1' P_{CH_4}}{1 + K_1 P_{CH_4}} \text{ where } k_1' = \frac{k_1}{K_2} \tag{16}$$

which explains that the reaction order is the zeroth-order with respect to CO_2 partial pressure. If P_{CO_2} is lower, that is, $K_2 P_{CO_2} \ll 1$, eq 15 will be approximated as

$$r = \frac{k_1 P_{CH_4} P_{CO_2}}{1 + K_1 P_{CH_4}} \tag{17}$$

Table 8. Kinetic Parameters for the Model of the Reaction Rate (Eq 15)

temp (°C)	k_1 (μmol/g_{cat}·s·kPa^2)	K_1 (kPa^{-1})	K_2 (kPa^{-1})
500	0.20	0.00082	4.3
550	0.29	0.015	2.3
600	0.24	0.023	0.80
650	0.25	0.020	0.50
700	0.32	0.035	0.43

The reaction is of the first-order with respect to CO_2 partial pressure. Similarly, at fixed CO_2 pressure, if $K_1 P_{CH_4} \ll 1$, eq 15 is simplified to

$$r = \frac{k_1 P_{CH_4} P_{CO_2}}{1 + K_2 P_{CO_2}} \tag{18}$$

Under this condition, the reaction is of the first-order with respect to CH_4 partial pressure.

The data were fit to the model (eq 15) and the best fit was obtained with the constants presented in Table 8. It is seen that the values of the equilibrium constant K_2 are generally higher than K_1, which explains the reason that activation energies for CO_2 consumption are greater than those of methane consumption. The reaction constant of k_1 is around 0.2−1.0 μmol/g_{cat}·s·kPa^2. Olsbye et al.[25] reported a value of 0.4 μmol/g_{cat}·s·kPa^2 for the Ni/La_2O_3−Al_2O_3 catalyst.

5. Conclusions

Several conclusions can be made on the basis of the investigations:

(1) Ni/γ-Al_2O_3 catalysts are effective for CO_2 reforming of methane, and the catalytic activity increases with increasing Ni loading. Optimum Ni loading, however, exists in terms of minimum coking. The 5 wt % Ni/γ-Al_2O_3 catalyst was found to be best for this reaction because it had higher conversion and much lesser magnitude of deactivation.

(2) Carbon deposition and nickel sintering are the major causes of Ni/γ-Al_2O_3 deactivation. However, active carbon species formed during the reaction play an important role in catalytic stability. XRD, XPS, and TEM studies revealed that two types of carbon deposits (oxidized and −C−C−) could form on the catalysts. Oxidized carbon presented in amorphous form exhibited higher reactivities toward gasification. Filamentous graphite exhibited less activity for gasification.

(3) The active sites of Ni/γ-Al_2O_3 catalysts for methane reforming with carbon dioxide are attributed to the reduced $NiAl_2O_4$, Ni particles, and Ni−C bonded intermediates. The role and extent of these active sites played in the reaction are the subjects of further research.

(4) Kinetic studies show that CO_2 reforming of methane over Ni/γ-Al_2O_3 could be described by applying a Langmuir−Hinshelwood-type expression. The activation energy for CO production was estimated to be 80 kJ/mol.

Acknowledgment

We acknowledge the financial support by the Australian Commonwealth Department of Education under the TIL program. We also thank Mr. F. Ausdley for conducting XRD measurements, Dr B. J. Wood for his help in XPS measurements, and Dr. J. Dremman for TEM analysis.

Literature Cited

(1) Wang, S.; Lu G. Q.; Millar, G. J. Carbon dioxide reforming of methane to produce synthesis gas over metal−supported catalysts: State-of-the art. *Energy Fuels* **1996**, *10*, 896−904.

(2) Edwards J. H.; Maitra, A. M. The chemistry of methane reforming with carbon dioxide and its current and potential application. *Fuel Process. Technol.* **1995**, *42*, 269−289.

(3) Nakamura, J.; Uchijima, T. Methane reforming with carbon dioxide. *Shokubai* **1993**, *35*, 478−484.

(4) Gadalla, A. M.; Bower, B. The role of catalyst support on the activity of nickel for reforming methane with CO_2. *Chem. Eng. Sci.* **1988**, *42*, 3049−3062.

(5) Zhang, Z. L.; Verykios, X. E. Carbon dioxide reforming of methane to synthesis gas over Ni/La_2O_3 catalysts. *Appl. Catal.* **1996**, *138*, 109−133.

(6) Seshan, K.; ten Barge, H. M.; Hally, W.; van Keulen, A. N. J.; Ross, J. R. H. Carbon dioxide reforming of methane in the presence of nickel and platinum catalysts supported on ZrO_2. *Stud. Surf. Sci. Catal.* **1994**, *81*, 285−290.

(7) Xu, H. Y.; Su, X. X.; Fan, Y. M.; Xu, G. L.; Liu, J. X.; Yu, W. G.; Zhou, P. H. Studies of reforming methane with carbon dioxide to produce synthesis gas, I. catalyst and its catalytic property. *Petrol. Chem. Eng.* **1992**, *21* (3), 147−153.

(8) Ruckenstein, E.; Hu, Y. H. Carbon dioxide reforming of methane over nickel/alkaline earth metal oxide catalysts. *Appl. Catal.* **1995**, *133*, 149−161.

(9) Ruckenstein, E.; Hu, Y. H. Role of support in CO_2 reforming of CH_4 to syngas over Ni catalysts. *J. Catal.* **1996**, *162*, 230−238.

(10) Takano, A.; Tagawa, T.; Goto, S. Carbon dioxide reforming of methane on supported nickel catalysts. *J. Chem. Eng. Jpn.* **1994**, *27*, 723−731.

(11) Kim, G. J.; Cho, D. S.; Kim, K. H.; Kim, J. H. The reaction of CO_2 with CH_4 to synthesise H_2 and CO over nickel-loaded Y-zeolite. *Catal. Lett.* **1994**, *28*, 41−52.

(12) Blom, R.; Dahl, I. M.; Slagtern, A.; Spjelkavik, A.; Tangstad, E. Carbon dioxide reforming of methane over lanthanum-modified catalysts in a fluidized-bed reactor. *Catal. Today.* **1994**, *21*, 535−543.

(13) Takayasu, O.; Soman, C.; Takegahara, Y.; Matsuura, I. Deactivation of Ni-catalysts and its prevention by mechanically mixing an oxide for the formation of reaction of CO+H_2 from CO_2+CH_4. *Stud. Surf. Sci. Catal.* **1994**, *88*, 281−188.

(14) Li, W. Y.; Xie, K. C.; Xie, S. C. Catalytic reaction of CO_2 and CH_4 for making syngas. *Coal Sci. Technol.* **1995**, *24*, 727−730.

(15) Wang S.; Lu, G. Q. CO_2 reforming of methane on Ni Catalysts: effects of the support phase and preparation technique. *Appl. Catal. B* **1998**, *16*, 269−277.

(16) Wang, S.; Zhu, H. Y.; Lu, G. Q. Preparation, characterisation and catalytic properties of clay-based nickel catalysts for methane reforming. *J. Colloid Interface Sci.* **1998**, *204*, 128−134.

(17) Chen, Y. G.; Ren, J. Conversion of methane and carbon dioxide into synthesis gas over alumina-supported nickel catalysts. Effect of Ni−Al_2O_3 interaction. *Catal. Lett.* **1994**, *29*, 39−48.

(18) Hu, Y. H.; Ruckenstein, E. An optimum NiO content in the CO_2 reforming of CH_4 with NiO/MgO solid solution catalysts. *Catal. Lett.* **1996**, *36*, 145−149.

(19) Zhang, Z. L.; Verykios, X. E. A stable and active nickel-based catalyst for carbon dioxide reforming of methane to synthesis gas. *J. Chem Soc., Chem. Commun.* **1995**, 71−72.

(20) Wang, S. Ph.D. Thesis, The University of Queensland, Queensland, Australia, 1998.

(21) Haines, P. J. *Thermal method of analysis principles, applications and problems*; London: Blackie Academic & Professional: U.K., 1995; p 1.

(22) Bradford, M. C. J.; Vannice, M. A. Catalytic reforming of methane with carbon dioxide over nickel catalysts II. Reaction kinetics. *Appl. Catal. A* **1996**, *142*, 97−122.

(23) Osaki, T.; Horiuchi, T.; Suzuki, K.; Mori, T. Kinetics, intermediates and mechanism for the CO_2-reforming of methane on supported nickel catalysts. *J. Chem. Soc., Faraday Trans.* **1996**, 92, 1627−1631.

(24) Rostrup-Nielsen, J. R.; Hansen, J. H. B. CO_2-reforming of methane over transition metals. *J. Catal.* **1993**, *144*, 38−49.

(25) Olsbye, U.; Wurzel, T.; Mleczko, L. Kinetics and reaction engineering studies of dry reforming of methane over a $Ni/La/Al_2O_3$ catalyst. *Ind. Eng. Chem. Res.* **1997**, *36*, 5180−5188.

(26) Takano, A.; Tagawa, T.; Goto, S. Carbon dioxide reforming of methane on supported nickel catalysts. *J. Chem. Eng. Jpn.* **1994**, *27*, 723−731.

(27) Al-Ubaid, A. S.; Wolf, E. E. Steam reforming of methane on reduced non-stoichimetric nickel aluminate catalysts. *Appl. Catal.* **1988**, *40*, 73−85.

(28) Al-Ubaid, A. S. Activity and stability of Ni spinel catalysts in water−methane reaction. *React. Kinet. Catal. Lett.* **1989**, *38*, 399−404.

(29) Murthy, I A. P. S.; Swamy, C. S. Catalytic behaviour of $NiAl_2O_4$ spinel upon hydrogen treatment. *J. Mater. Res.* **1993**, *28*, 1194−1198.

(30) Dissanayake, D.; Rosynek, M. P.; Kharas, K. C. C.; Lunsford, J. H. Partial oxidation of methane to carbon monoxide and hydrogen over a Ni/Al_2O_3 catalyst. *J. Catal.* **1991**, *132*, 117−127.

(31) Chen, I.; Shiue, D. W. Reduction of nickel-alumina catalysts. *Ind. Eng. Chem. Res.* **1988**, *27*, 429−434.

(32) Zhang, Z. L.; Tsipouriari, V. A.; Efstathiou, A. M.; Verykios, X. E. Reforming of methane with carbon dioxide to synthesis gas over supported rhodium catalysts, I. Effect of support and metal crystallite size on reaction activity and deactivation characteristics. *J. Catal.* **1996**, *158*, 51−63.

(33) York, A. P. E.; Claridge, J. B.; Brungs, A. J.; Tsang, S. C.; Green, M. H. Molybdenum and tungsten carbides as catalysts for the conversion of methane to synthesis gas using stoichimetric feedstocks. *Chem. Commun.* **1997**, 39−40.

(34) Efstathiou, A. M.; Kladi, A.; Tsipouriari, V. A.; Verykios, X. E. Reforming of methane with carbon dioxide to synthesis gas over supported rhodium catalysts II. A steady-state tracing analysis: mechanistic aspects of the carbon and oxygen reaction pathways to form CO. *J. Catal.* **1996**, *158*, 64−75.

(35) Kroll, V. C. H.; Swaan, H. M.; Mirodatos, C. Methane reforming reaction with carbon dioxide over Ni/SiO_2 catalyst I. Deactivation studies. *J. Catal.* **1996**, *161*, 409−422.

(36) Mark, M. F.; Maier, W. F. Active surface carbon—A reactive intermediate in the production of synthesis gas from methane and carbon dioxide. *Angew. Chem., Int. Ed. Engl.* **1993**, *33*, 1657−1660.

(37) Solymosi, F.; Kutsan, G.; Erdohelyi, A. Catalytic reaction of methane with carbon dioxide over alumina-supported platinum metals. *Catal. Lett.* **1991**, *11*, 149−156.

(38) Lercher, J. A.; Bitter, J. H.; Hally, W.; Niessen, W.; Seshan, K. Design of stable catalysts for methane-carbon dioxide reforming. *Stud. Surf. Sci. Catal.* **1996**, *101*, 463−472.

(39) Mikhailova, A. V.; Alekseev, A. M.; Beskov, V. S. Formation of filamentous carbon in the reaction of carbon dioxide with methane on nickel catalyst. *Theor. Found. Chem. Eng.* **1996**, *30*, 174−178.

(40) de Bokx, P. K.; Kock, A. J. H.; Boellaad, E.; Elop, W.; Geus, J. W. The formation of filamentous carbon on iron and nickel catalysts I. Thermodynamics. *J. Catal.* **1985**, *96*, 454−467.

(41) Shi, J. L.; Zhang, J. Y.; Liu, Z. Study of stepwise syngas production from methane and carbon dioxide on supported nickel catalyst. *Nat. Gas Chem. Eng.* **1995**, *20* (2), 14−18.

(42) Goula, M. A.; Lemonidou, A. A.; Efstathiou, A. M. Characterisation of carbonaceous species formed during reforming of CH_4 with CO_2 over $Ni/CaO−Al_2O_3$ catalysts studied by various transient techniques. *J. Catal.* **1996**, *161*, 626−640.

(43) Swaan, H. M.; Kroll, V. C. H.; Martin, G. A.; Mirodatos, C. Deactivation of supported nickel catalysts during the reforming of methane by carbon dioxide. *Catal. Today.* **1994**, *21*, 571−578.

(44) Bartholomew, C. H. Carbon deposition in steam reforming and methanation. *Catal. Rev. Sci. Eng.* **1982**, *24*, 67−112.

(45) Beellaard, E.; de Bokx, P. K.; Kock, A. J. H. M.; Geus, J. W. The formation of filamentous carbon on iron and nickel catalysts. III. Morphology. *J. Catal.* **1986**, *96*, 481−490.

(46) Rostrup-Nielsen, J. R. Catalytic steam reforming. In *Catalysis Science and Technology*; Anderson, J. R., Boudart, M., Eds.: Springer: London, 1984: Vol. 5, pp 1−117.

(47) Baker, R. T. K. Catalytic growth of carbon filaments. *Carbon* **1989**, *27*, 315−323.

(48) Zhang, Z. L.; Verykios, X. E. Mechanistic aspects of carbon dioxide reforming of methane to synthesis gas over Ni catalysts. *Catal. Lett.* **1996**, *38*, 175−179.

(49) Wang, H. Y.; Au, C. T. CH_4/CD_4 isotope effects in the carbon dioixde reforming of methane to syngas over SiO_2-supported nickel catalysts. *Catal. Lett.* **1996**, *38*, 77−79.

(50) Slagtern, A.; Olsbye, U.; Blom, R.; Dahl, I. M. The influence of rare earth oxides on Ni/Al_2O_3 catalysts during CO_2 reforming of CH_4. *Stud. Surf. Sci. Catal.* **1997**, *107*, 497−502.

(51) Aparicio, L. M. Transient isotopic studies and microkinetic modeling of methane reforming over nickel catalysts. *J. Catal.* **1997**, *165*, 262−274.

(52) Hu, Y. H.; Ruckenstein, E. Transient Response analysis via a broadened pulse combined with a step change or an isotopic pulse: Application to CO_2 reforming of methane over NiO/SiO_2. *J. Phys. Chem. B* **1997**, *101*, 7563−7565.

(53) Ruckenstein, E.; Hu, Y. H. Role of lattice oxygen during CO_2 reforming of methane over NiO/MgO solid solutions. *Catal. Lett.* **1998**, *51*, 183−185.

(54) Osaki, T.; Masuda, H.; Mori, T. Intermediate hydrocarbon species for the $CO_2−CH_4$ reaction on supported Ni catalysts. *Catal. Lett.* **1994**, *29*, 33−37.

(55) Zhang, Z. L.; Verykios, X. E. Carbon dioxide reforming of methane to synthesis gas over supported Ni catalysts. *Catal. Today.* **1994**, *21*, 589−595.

(56) Mark, M. F.; Mark, F.; Maier, W. F. Reaction kinetics of the CO_2 reforming of methane. *Chem. Eng. Technol.* **1997**, *20*, 361−370.

Received for review July 30, 1998
Revised manuscript received March 9, 1999
Accepted March 11, 1999

IE980489T